ARTICLE   OPEN

In situ XPS investigation of the X-ray-triggered decomposition of perovskites in ultrahigh vacuum condition

Wei-Chun Lin [1,2 ✉], Wei-Chun Lo[2], Jun-Xian Li[2], Yi-Kai Wang[2], Jui-Fu Tang[1] and Zi-Yun Fong[1]

X-ray photoelectron spectroscopy (XPS) has been used to investigate the composition of perovskite films upon exposure to different environmental factors, such as moisture, heat, and UV light. However, few research studies have determined that the X-ray itself could cause damage to the perovskite crystals. In this study, the X-ray-induced degradation of $CH_3NH_3PbI_3$ perovskite films was investigated via XPS within an in situ ultrahigh vacuum system. It is demonstrated that fresh methylammonium lead iodine contains Pb^{2+} without the initial existence of Pb^0. The Pb^0 signal was discovered after a few hours of soft X-ray exposure, which indicates that the $CH_3NH_3PbI_3$ perovskite structure undergoes a decomposition process to form metallic Pb. In addition, the nitrogen content was found to be significantly decreasing in the first hour of X-ray exposure. The discovery of the X-ray-induced chemical state change and the volatile methylamine of perovskite crystals could be further applied as an indicator for the field of X-ray sensors or detectors.

npj Materials Degradation (2021)5:13 ; https://doi.org/10.1038/s41529-021-00162-9

INTRODUCTION

Lead-based organic–inorganic hybrid perovskites have recently attracted much attention as superior light-harvesting materials and offer high power conversion efficiencies of >25% for certified cells[1]. $CH_3NH_3PbI_3$ perovskite has diverse advantages, such as a high absorption coefficient, an ideal band gap energy of ~1.5 eV, high carrier mobility, and a defect tolerance[2–6]. These perovskite solar cells (PSCs) could be fabricated as mesoscopic or planar structured devices[7–12]. Initially, the perovskite films in mesoscopic PSCs were made using a precursor by a one-step deposition method[13], which led to an unstable film morphology and large variations in the cell efficiency. A sequential deposition method was then developed to control the morphology of the perovskite films, which led to a better device performance and repeatability[10]. In subsequent studies, various fabrication techniques, such as dual-source vapor deposition[14], a vapor-assisted solution process[15], a solvent-assisted fast crystallization method[16], and low-temperature casting[17], were proposed to produce PSCs with planar structures. Despite the major progress in the fabrication techniques and device performance achieved over the last few years, PSCs need to overcome several technical concerns before their successfully widespread commercial use is achieved. One of the most significant concerns for PSCs is their long-term stability[18,19]. The stability issues of PSCs should be urgently addressed to achieve excellent reproducibility and a long lifetime for device operation. Different stress conditions (light exposure, air/moisture environment, etc.) play individual roles in accelerating the degradation rate relative to degradation under standard operating conditions. One of the most straightforward aging tests is the light exposure experiment. Recently, Misra et al. reported the accelerated degradation testing of perovskite films under exposure to concentrated sunlight of 100 suns[20]. Farooq et al. also studied the ultraviolet light-induced degradation of PSCs[21]. Among the various forms of electromagnetic radiation, X-rays are mostly used to study the interactions of the above-mentioned stress conditions with perovskite films. For example, X-ray diffraction (XRD) was used to characterize the perovskite crystals[7,14,22–24]. X-ray photoelectron spectroscopy (XPS) was used to confirm the elemental composition[25,26] and to study the decomposition process of the device through depth profiling[27]. However, only a few research groups have investigated the interaction of perovskite films upon exposure to X-rays[28]. Here, we demonstrated the use of X-ray exposure for $CH_3NH_3PbI_3$ perovskite degradation testing. The X-ray source in the XPS system was used to hit the perovskite films and in situ detect the elemental composition and the chemical states after the specimen was aged. In this study, it was found that Pb^0, not the original state of perovskite (Pb^{2+}), was generated by 20-min X-ray exposure. The chemical state of C1s was altered by the X-ray exposure from the C-N bond (286 eV) to C-C bond (284.9 eV) as well. The XPS results showed that the perovskite films underwent different decomposed reactions, which were measured by XRD.

RESULTS AND DISCUSSION

XRD and surface morphology

The $CH_3NH_3PbI_3$ perovskite was deposited on indium tin oxide (ITO) substrates via a sequential deposition method without a hole or an electron transporting layer to exclude possible factors from other materials. The XRD patterns in Fig. 1a confirm the presence of PbI_2 after 40 h of X-ray exposure (red curve). The blue curve illustrates the specimen stored in ambient conditions (relative humidity (R.H.) ~40%, room temperature ~25 °C) in the dark as a reference to discuss chemical state in the next section. Scanning electron microscopy (SEM) was used to examine the film morphology of the fresh samples and X-ray-exposed samples. The inset SEM image in Fig. 1a demonstrates the aged samples under ambient conditions for 4 weeks, where the crystal boundary was altered significantly, and many holes between grains were observed. The fresh sample shows the dense and coarse-grained morphology with a grain size of ~200 nm, indicating the uniform coverage of the perovskite crystal above the ITO substrate (Fig.

[1]Department of Photonics, National Sun Yat-sen University, Kaohsiung, Taiwan, ROC. [2]Department of Materials Science and Engineering, Feng Chia University, Taichung, Taiwan, ROC. ✉email: wclin@mail.nsysu.edu.tw
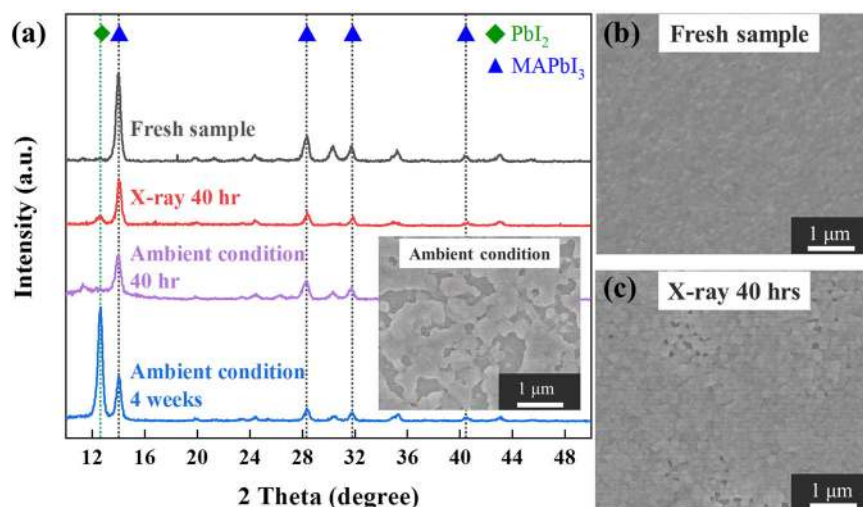
Fig. 1 Crystallinity and surface morphology of perovskite films. a XRD patterns of perovskite films with different storage conditions. The inset SEM image in Fig. 1a is the specimen under ambient conditions for 4 weeks. SEM images of the sample treated with **b** 0-h and **c** 40-h X-ray irradiation.

1b). In contrast, perovskite grains receiving X-ray exposure for 40 h contain a few pinhole defects in their coating, which exposes the underneath ITO substrate (Fig. 1c). The reason for pinhole generation is due to the decomposition of perovskite crystal upon X-ray exposure. Hence, further in situ XPS investigation regarding the surface chemistry of perovskite is crucial for understanding the origin of the pinhole formation.
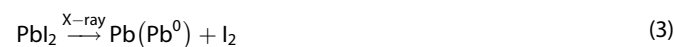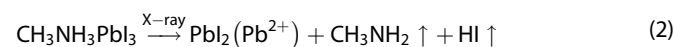
XPS surface spectra obtained with different X-ray exposure durations

The ITO/perovskite samples experiencing different storage conditions were examined by XPS. The survey spectrum of a fresh sample (no X-ray exposure before measurement) represents the typical peaks of perovskite crystals, such as the Pb4f, C1s, N1s, and I3d peaks (Supplementary Fig. 1). Due to the limited detection depth (~6–10 nm), the signals of In3d, Sn3d, and O1s (ITO) were not observed. To avoid artifacts caused by sputtering, only the surface region (~6 nm) was further fine scanned to confirm the chemical state of each element. The elemental fine scan was inevitably performed by exposing an $\sim500 \times 500\ \mu m^2$ area of the fresh sample to X-rays for ~20 min during the measurement. Unless otherwise stated, the X-ray exposure time mentioned in this section considers X-ray exposure during the measurement.

Figure 2 demonstrates the XPS fine scan spectra of C1s, N1s, O1s, Pb4f, and I3d obtained with different X-ray irradiation conditions before the measurement. Note that the fresh sample and the sample stored in an ambient environment (R.H. ~40% in the dark) are both exposed to X-rays during the XPS measurements (~20 min). The solid black curve in Fig. 2a represents a typical C spectrum of a fresh perovskite sample, with a primary peak at ~286 eV (C-N bond) and a shoulder peak at ~284.9 eV (C-C bond)[29]. The blue dashed curve in Fig. 2a shows a spectrum of the control sample aged in ambient conditions for 4 weeks. The double peaks of the ambient condition spectrum (blue dash curve) indicate that the perovskite crystal was gradually decomposed due to the increase in the intensity of the C-C bond peak. Similar C1s double peaks were observed for the specimen upon X-ray exposure for 9 h (orange curve). The peak attributed to the C-N bond at 286 eV disappeared and became a shoulder if the specimen was further irradiated by X-rays for 14 h (green curve). Figure 2b illustrates the background-subtracted N spectrum of each sample, and a significantly decreasing intensity of nitrogen

due to X-ray irradiation enduring several hours is observed. It is noticed that the N intensity of the ambient condition sample is higher than that of the samples exposed to X-rays. The inset of Fig. 2b shows the O1s spectra, indicating that only the ambient condition specimen has a reasonable signal/noise ratio. It proves that the X-ray exposed specimen stored in the ultrahigh vacuum (UHV) condition, which is not damaged by oxygen. The result of the N spectra is consistent with the degradation mechanisms published by different groups, indicating the slow leaching and vaporization process of CH_3NH_2, which is due to the exposure of moisture[28,30]. The Pb4f spectra in Fig. 2c illustrates the variety of peak widths observed for each specimen. The specimen stored in ambient conditions exhibits an extra small peak at ~136.2 eV (blue dash curve), indicating that metallic Pb^0 was formed due to the long-term exposure to moisture (~R.H. 40%). It can be noticed that the Pb4f peak of the sample became broader than that of the fresh sample (black curve) with increasing the X-ray exposure duration (orange and green curves). It is clear that the perovskite underwent a decomposition process during X-ray irradiation.

Two X-ray-induced decomposition routes occur simultaneously to produce $PbI_{2(s)}$, $CH_3NH_3I_{(s)}$, $CH_3NH_{2(g)}$, and $HI_{(g)}$, as shown in the reactions 1 and 2 below. The decomposed lead iodide (PbI_2) maintains a similar chemical state to the chemical state of original perovskite (Pb^{2+}). Furthermore, metallic Pb (Pb^0) will be produced if the duration of X-ray irradiation is prolonged (reaction 3), resulting in the broader Pb peak in Fig. 2c. This outcome suggested that a small portion of Pb shifts its chemical state from Pb^{2+} (138 eV) to Pb^0 (136.2 eV)[28,29]. The iodine spectrum in Fig. 2d shows broad peaks from the X-ray-degraded samples as well, which indicates that $CH_3NH_3PbI_3$ loses iodine from the perovskite crystal structure in the form of I_2 or HI (reaction 2 and 3)[28].

$$CH_3NH_3PbI_3 \xrightarrow{X-ray} PbI_2\left(Pb^{2+}\right) + CH_3NH_3I \tag{1}$$

$$CH_3NH_3PbI_3 \xrightarrow{X-ray} PbI_2\left(Pb^{2+}\right) + CH_3NH_2 \uparrow + HI \uparrow \tag{2}$$

$$PbI_2 \xrightarrow{X-ray} Pb\left(Pb^0\right) + I_2 \tag{3}$$

To confirm the process of the chemical change by X-rays, the $Pb4f_{7/2}$ and $I3d_{5/2}$ core-level spectra were collected by performing in situ XPS measurements after X-ray irradiation (Fig. 3). The specimen was measured at 2-h intervals initially, and then 1-h
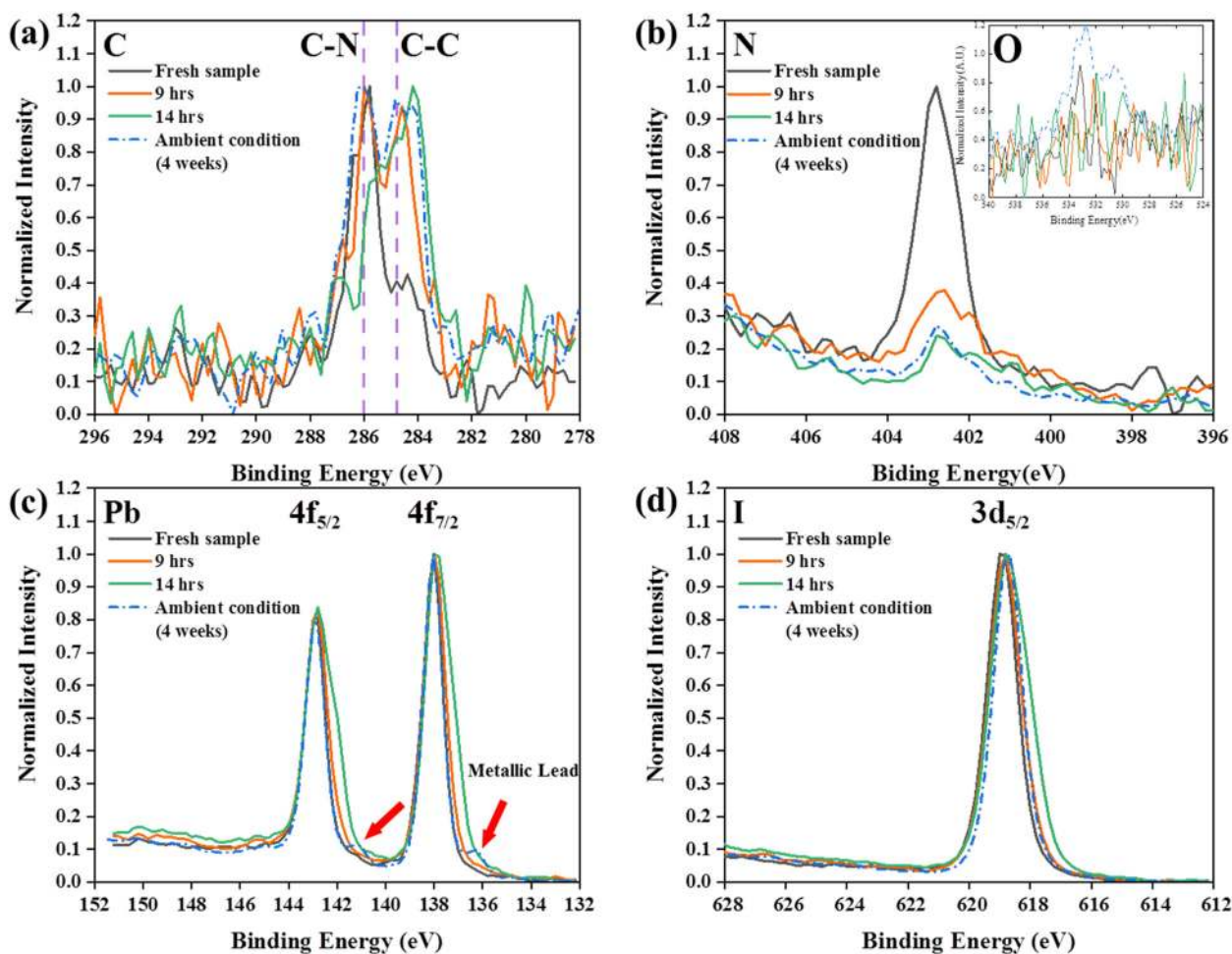
Fig. 2 Surface chemistry of the primary elements. XPS spectra of **a** carbon, **b** nitrogen, **c** lead and **d** iodine peaks upon exposure to the X-ray source used in XPS for 20 min (fresh sample), and 9 h, 14 h and those of the sample stored in ambient conditions for 4 weeks (w.o. X-ray exposure). The inset figure in the N spectrum illustrates the oxygen spectrum.

intervals were used after 10 h of exposure for the rapid observation of the spectrum. As shown in Fig. 3a, the curve shape of the Pb4f$_{7/2}$ spectrum is conserved for the specimen exposed to 2, 4, and 6 h. The peak width was then broadened over time from 8 to 14 h of X-ray exposure (Fig. 3a, b). A variety of Pb4f$_{7/2}$ peak widths was confirmed with the normalized spectra shown in Supplementary Fig. 2. A similar phenomenon has been observed in the I3d$_{5/2}$ spectra over time, as shown in Fig. 3c, d. The normalized I3d$_{5/2}$ spectra in Supplementary Fig. 3 also proves the wider full-width at half-maximum (FWHM) over the irradiation time. The broadened peaks of Pb4f$_{7/2}$ and I3d$_{5/2}$ indicated that metallic Pb (Pb^0) and I$_2$ crystals were formed under long-term X-ray exposure (reaction 3).

XPS elemental composition of the X-ray-degraded perovskite films

The elemental ratio and relative atomic concentration of C, N, Pb, and I on the CH$_3$NH$_3$PbI$_3$ perovskite surface in ambient conditions (R.H. ~40%, 25 °C in the dark) and under X-ray irradiation were both examined under UHV conditions, as shown in Fig. 4a, b, respectively. The initial elemental ratio (C:N:Pb:I) of fresh CH$_3$NH$_3$PbI$_3$ in the dark was 1.8:1.3:1:2.4 (Fig. 4a), which is close to the stoichiometric value. The slightly high amount of iodine observed in the surface-sensitive analysis could be attributed to the excessive methylammonium iodide present on the top surface

due to the two-step preparation of the perovskite films[30]. The detailed composition of the control specimen was listed in Supplementary Table 1. In the following 14 h of X-ray irradiation in the XPS main chamber (in the dark), the intensity of the N1s peak decreases over time, which can be correlated with the outgassing of methylamine (CH$_3$NH$_2$) produced via reaction 2 (Fig. 4b). The slight increase in the lead and iodine contents could be attributed to the residual PbI$_2$ left on the surface under UHV and X-ray exposure conditions. The oxygen content can be neglected due to the small amount observed under both conditions. Note that the amount of nitrogen decrease significantly in the first hour of X-ray exposure. Meanwhile, it takes ~14 h for the nitrogen of a fresh specimen to drop from ~20 to 14% in the ambient condition. The increase in the lead and iodine content with increasing X-ray exposure times also proved that the volatile methylamine disappeared. In summary, the change in the perovskite film composition from ambient conditions and X-ray exposure is different (Supplementary Tables 1 and 2). The X-ray exposure causes faster decomposition of the perovskite film than the ambient conditions. In contrast, the composition of the perovskite film stored in the ambient condition does not obviously exhibit elemental fluctuations after 8 h of proper storage. The X-ray-triggered decomposition process of the perovskite crystals was accompanied with the production of methylamine, which results
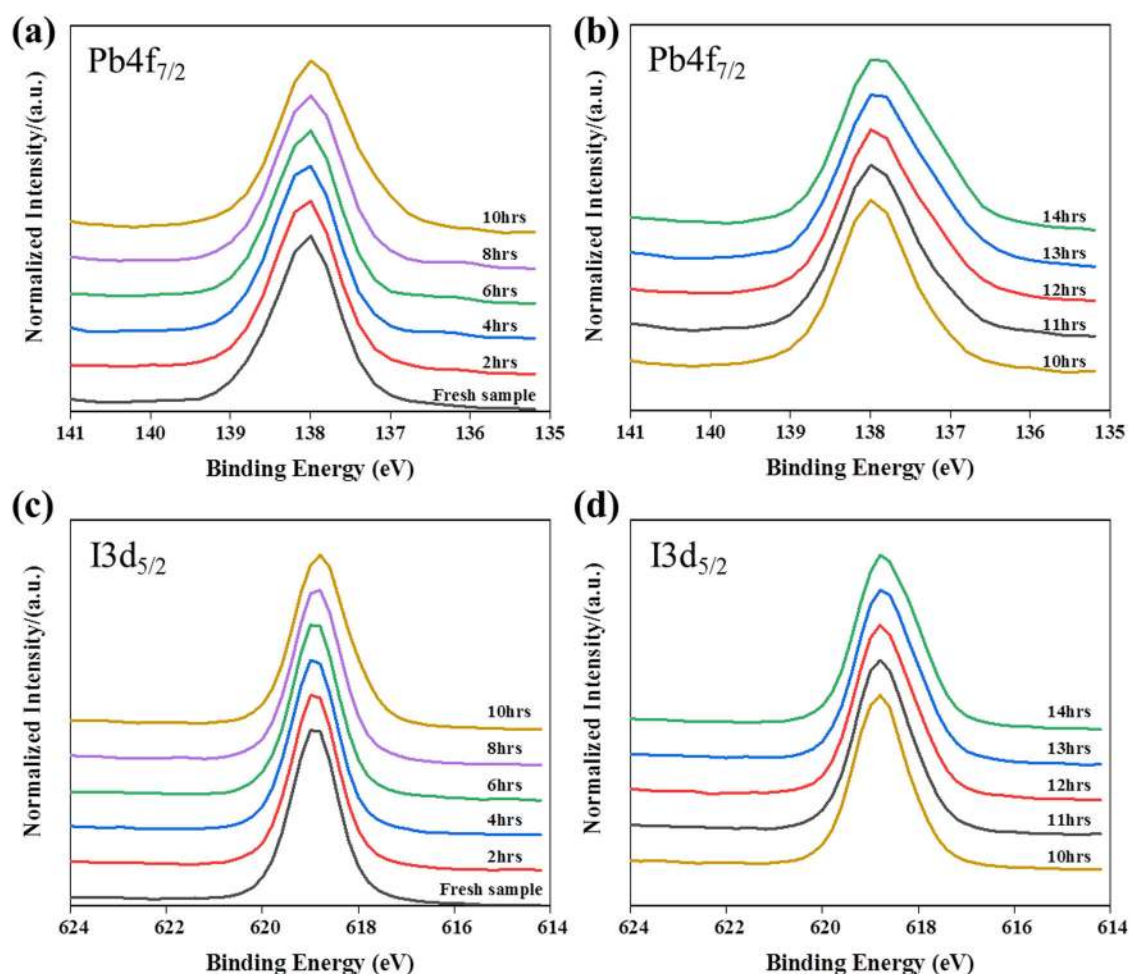
Fig. 3   Study of chemical states of lead and iodine under X-ray illumination for 0–14 h. XPS spectra of $Pb4f_{7/2}$ (**a**, **b**) and $I3d_{5/2}$ (**c**, **d**) with X-ray exposure from 0 to 14 h. The duration of the X-ray exposure in the figure do not include the X-ray irradiation during XPS measurements. The X-ray exposure during the measurement of the each sample was limited to <20 min.

in an elemental quantity change within 1 h. The elemental fluctuation is a useful indicator for detecting X-rays.

In summary, X-ray irradiation of the $CH_3NH_3PbI_3$ film results in the chemical state change of the C1s spectrum and the formation of metallic lead, which indicates the decomposition of the perovskite crystals. The disappearance of the N1s peak and the broadening of the FWHM of the I3d peak during X-ray exposure proves the removal of organic components from the perovskite film, resulting in the formation of PbI_2 (Pb^{2+}), Pb (Pb^0), and I_2. These in situ XPS findings in vacuum, i.e., in an inert atmosphere, show that perovskite degrades primary due to X-ray irradiation. Therefore, the characterization of perovskite films using X-ray techniques should be carefully grasped between research quality and artifact. As for the application, the surface composition change could be an indicator about the damage of perovskite films upon exposure to X-ray.

METHODS
Preparation of perovskite sample
To emphasize the influence of X-ray irradiation on perovskite films, the charge transporting layer was removed to simplify the experimental parameters. ITO-based perovskite samples were fabricated with a device architecture (ITO/$CH_3NH_3PbI_3$) similar to that of the commonly used planar $CH_3NH_3PbI_3$ structure via sequential deposition, which has been published elsewhere.

Sample characterization
XRD measurements were conducted with a Bruker D8 Discover instrument operated with Cu Kα radiation. Unless otherwise stated, the X-ray exposure time was limited to <20 min during each XRD measurement. Images of the film morphology were obtained using an FEI Nova nanoSEM 200 field emission scanning electron microscope operated at 15 kV without a conductive overcoat under a low vacuum (0.5 Torr) environment. Low vacuum mode was used to avoid sample charge-up during imaging.

XPS measurements. The XPS spectra were recorded with a PHI 5000 VersaProbe system (ULVAC-PHI, Chigasaki, Japan). The microfocused Al Kα X-rays (25 W, 100 μm) and the analyzer scanned an area of 500×500 μm^2. Identically, these monochromated soft X-rays were used to irradiate the perovskite samples with various durations for the measurement. The take-off angle of the photoelectron was fixed at 45°. Unless otherwise stated, the XPS measurements were performed with a dual-beam charge neutralizer for charge compensation. Samples were treated with X-ray exposure under UHV conditions in the dark in the XPS main chamber. The chamber pressures during X-ray exposure and XPS measurements are 8×10^{-6} and 1×10^{-5} Pa, respectively. The X-ray exposure of the fresh sample was limited to <20 min during the measurement, and all the measuring procedures were performed in the dark.

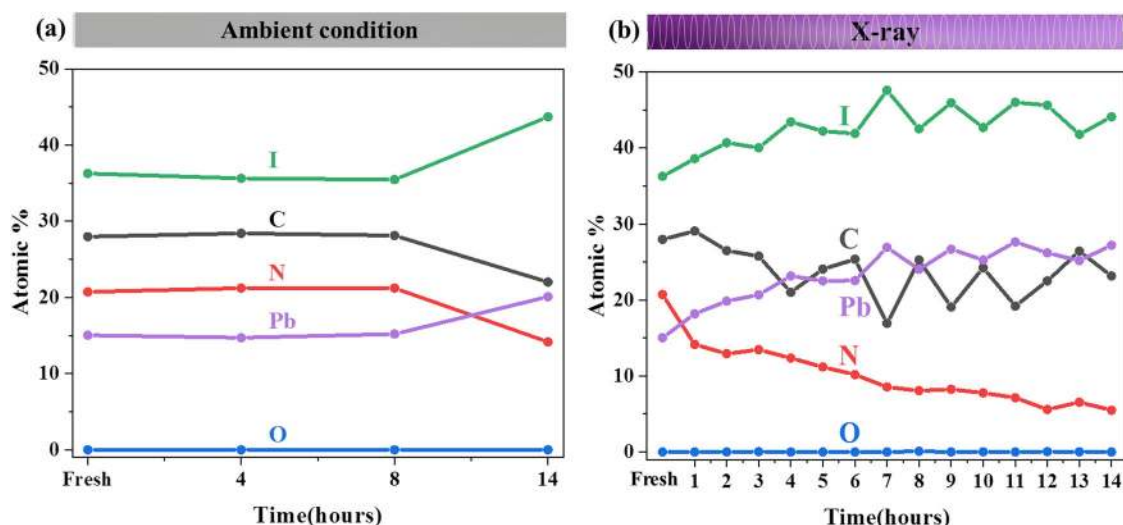**Fig. 4 Surface elemental ratio of MAPbI$_3$ under dark and X-ray. a** Surface composition of CH$_3$NH$_3$PbI$_3$ perovskite under ambient and **b** X-ray irradiation conditions over time in ultrahigh vacuum.

REFERENCES

1. Yan, Y. et al. Best research-cell efficiency chart. Photovoltaic research. NREL. *J. Am. Chem. Soc.* **5**, 1–8 (2020).
2. Wehrenfennig, C., Liu, M., Snaith, H. J., Johnston, M. B. & Herz, L. M. Charge-carrier dynamics in vapour-deposited films of the organolead halide perovskite CH$_3$NH$_3$PbI$_{3-x}$Cl$_x$. *Energy Environ. Sci.* https://doi.org/10.1039/c4ee01358a (2014).
3. Savenije, T. J. et al. Thermally activated exciton dissociation and recombination control the carrier dynamics in organometal halide perovskite. *J. Phys. Chem. Lett.* https://doi.org/10.1021/jz500858a (2014).
4. Wehrenfennig, C., Eperon, G. E., Johnston, M. B., Snaith, H. J. & Herz, L. M. High charge carrier mobilities and lifetimes in organolead trihalide perovskites. *Adv. Mater.* https://doi.org/10.1002/adma.201305172 (2014).
5. Ponseca, C. S. et al. Organometal halide perovskite solar cell materials rationalized: ultrafast charge generation, high and microsecond-long balanced mobilities, and slow recombination. *J. Am. Chem. Soc.* https://doi.org/10.1021/ja412583t (2014).
6. Xing, G. et al. Long-range balanced electron-and hole-transport lengths in organic-inorganic CH$_3$NH$_3$PbI$_3$. *Science* **342**, 344–347 (2013).
7. Raga, S. R. et al. Influence of air annealing on high efficiency planar structure perovskite solar cells. *Chem. Mater.* https://doi.org/10.1021/cm5041997 (2015).
8. Ball, J. M., Lee, M. M., Hey, A. & Snaith, H. J. Low-temperature processed meso-superstructured to thin-film perovskite solar cells. *Energy Environ. Sci.* **6**, 1739 (2013).
9. Bai, S. et al. High-performance planar heterojunction perovskite solar cells: preserving long charge carrier diffusion lengths and interfacial engineering. *Nano Res.* **7**, 1749–1758 (2014).
10. Burschka, J. et al. Sequential deposition as a route to high-performance perovskite-sensitized solar cells. *Nature* https://doi.org/10.1038/nature12340 (2013).
11. Heo, J. H. et al. Efficient inorganic–organic hybrid heterojunction solar cells containing perovskite compound and polymeric hole conductors. *Nat. Photonics* **7**, 486–491 (2013).
12. Han, Y. et al. Degradation observations of encapsulated planar CH$_3$NH$_3$PbI$_3$ perovskite solar cells at high temperatures and humidity. *J. Mater. Chem. A* **3**, 8139–8147 (2015).
13. Kojima, A., Teshima, K., Shirai, Y. & Miyasaka, T. Organometal halide perovskites as visible-light sensitizers for photovoltaic cells. *J. Am. Chem. Soc.* https://doi.org/10.1021/ja809598r (2009).
14. Liu, M., Johnston, M. B. & Snaith, H. J. Efficient planar heterojunction perovskite solar cells by vapour deposition. *Nature* https://doi.org/10.1038/nature12509 (2013).
15. Chen, Q. et al. Planar heterojunction perovskite solar cells via vapor-assisted solution process. *J. Am. Chem. Soc.* https://doi.org/10.1021/ja411509g (2014).
16. Xiao, M. et al. A fast deposition-crystallization procedure for highly efficient lead iodide perovskite thin-film solar cells. *Angew. Chem. Int. Ed.* https://doi.org/10.1002/anie.201405334 (2014).
17. Yella, A., Heiniger, L. P., Gao, P., Nazeeruddin, M. K. & Grätzel, M. Nanocrystalline rutile electron extraction layer enables low-temperature solution processed perovskite photovoltaics with 13.7% efficiency. *Nano Lett.* https://doi.org/10.1021/nl500399m (2014).
18. Grätzel, M. The light and shade of perovskite solar cells. *Nat. Mater.* **13**, 838–842 (2014).
19. Green, M. A., Ho-Baillie, A. & Snaith, H. J. The emergence of perovskite solar cells. *Nat. Photonics* **8**, 506–514 (2014).
20. Misra, R. K. et al. Temperature- and component-dependent degradation of perovskite photovoltaic materials under concentrated sunlight. *J. Phys. Chem. Lett.* https://doi.org/10.1021/jz502642b (2015).
21. Farooq, A. et al. Spectral dependence of degradation under ultraviolet light in perovskite solar cells. *ACS Appl. Mater. Interfaces* https://doi.org/10.1021/acsami.8b03024 (2018).
22. Zhou, H. et al. Interface engineering of highly efficient perovskite solar cells. *Science* https://doi.org/10.1126/science.1254050 (2014).
23. Niu, G., Guo, X. & Wang, L. Review of recent progress in chemical stability of perovskite solar cells. *J. Mater. Chem. A* **3**, 8970–8980 (2014).
24. Leijtens, T. et al. Overcoming ultraviolet light instability of sensitized TiO$_2$ with meso-superstructured organometal tri-halide perovskite solar cells. *Nat. Commun.* **4**, 2885 (2013).
25. Ahmad, Z. et al. Instability in CH$_3$NH$_3$PbI$_3$ perovskite solar cells due to elemental migration and chemical composition changes. *Sci. Rep.* https://doi.org/10.1038/s41598-017-15841-4 (2017).
26. Mierwaldt, D. et al. In situ XANES/XPS investigation of doped manganese perovskite catalysts. *Catalysts* https://doi.org/10.3390/catal4020129 (2014).
27. Lin, W. C. et al. Interpenetration of CH$_3$NH$_3$PbI$_3$ and TiO$_2$ improves perovskite solar cells while TiO$_2$ expansion leads to degradation. *Phys. Chem. Chem. Phys.* https://doi.org/10.1039/c7cp03116e (2017).
28. McGettrick, J. D. et al. Sources of Pb(0) artefacts during XPS analysis of lead halide perovskites. *Mater. Lett.* https://doi.org/10.1016/j.matlet.2019.04.081 (2019).
29. Chen, S., Solanki, A., Pan, J. & Sum, T. C. Compositional and morphological changes in water-induced early-stage degradation in lead halide perovskites. *Coatings* https://doi.org/10.3390/coatings9090535 (2019).
30. Lin, W. C., Chang, H. Y., Abbasi, K., Shyue, J. J. & Burda, C. 3D in situ ToF-SIMS imaging of perovskite films under controlled humidity environmental conditions. *Adv. Mater. Interfaces* https://doi.org/10.1002/admi.201600673 (2017).

AUTHOR CONTRIBUTIONS

COMPETING INTERESTS

The authors declare no competing interests.

ADDITIONAL INFORMATION

Supplementary information The online version contains supplementary material available at https://doi.org/10.1038/s41529-021-00162-9.

Correspondence and requests for materials should be addressed to W.-C.L.

Reprints and permission information is available at http://www.nature.com/reprints

Publisher's note Springer Nature remains neutral with regard to jurisdictional claims in published maps and institutional affiliations.